ACS Photonics

Letter

Cite This: ACS Photonics 2018, 5, 1863−1870

Wavelength-Dependent Third-Harmonic Generation in Plasmonic Gold Nanoantennas: Quantitative Determination of the d-Band Influence

Joachim Krauth,* Harald Giessen, and Mario Hentschel

4th Physics Institute and Research Center SCoPE, University of Stuttgart, Pfaffenwaldring 57, 70569 Stuttgart, Germany

Supporting Information

ABSTRACT: Plasmonic gold nanoantennas are highly efficient nanoscale nonlinear light converters. The nanoantennas provide large resonant light interaction cross sections as well as strongly enhanced local fields. The actual frequency conversion, however, takes places inside the gold volume and is thus ultimately determined by the microscopic gold nonlinearity, which has been found to significantly surpass common bulk nonlinear materials. While the influence of the nanoantenna geometry and hence the plasmonic resonance has been studied in great detail, only little attention has been paid to the microscopic material nonlinearity. Here we show that the microscopic third-order nonlinearity of gold is in fact a resonant one by virtue of interband transitions between the d- and sp-bands. Utilizing a large set of resonant nanoantennas and a fiber-feedback optical parametric oscillator as a broadband-tunable light source, we show that the radiated third-harmonic signals significantly increase at the onset of interband transitions, namely, as soon as the third harmonic becomes resonant with allowed interband transitions. With the help of an anharmonic oscillator model and independent reference measurements on a gold film we can unambiguously demonstrate that the observed third-harmonic increase is related to a strongly wavelength-dependent microscopic third-order gold nonlinearity, which is additionally underlined by quantitative agreement between simulation and measurement. This additional tuning parameter allows further manipulation and optimization of nonlinear nanoscale systems and thus renders the investigation of other plasmonic materials, especially with interband transitions located in the ultraviolet range, highly intriguing.

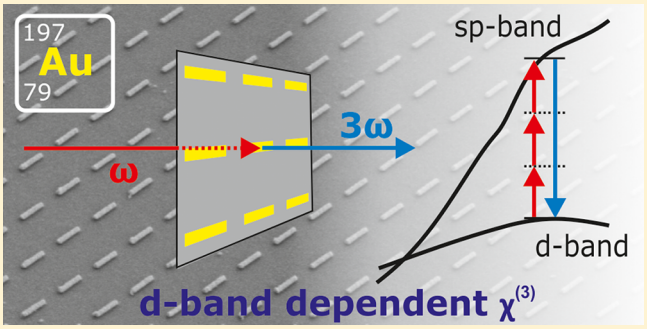

KEYWORDS: *nonlinear plasmonics, spectroscopy, nonlinear material susceptibility, gold, interband transitions*

How does one manipulate or even tailor the nonlinear optical properties of matter? This question has intrigued researchers for decades due to manifold applications involving nonlinear effects, such as frequency conversion and mixing, self-focusing, self-phase modulation, and optical solitons.[1,2] Moreover, nonlinear spectroscopy and imaging have been widely used to investigate properties and dynamics of matter, particularly on surfaces.[3,4] In more recent times, researchers began studying plasmonic systems for this purpose due to their intrinsic tunability and manipulability.[5,6] A plasmon, the collective oscillation of the quasi-free conduction electrons in metal nanostructures, is characterized by large resonant light interaction cross sections and strongly enhanced local fields, which both are expected to efficiently drive nonlinear conversion processes.[7] Moreover, due to advances in micro- and nanofabrication, the design, layout, and material composition and, consequently, the optical response of these systems can be tailored nearly at will,[8,9] in stark contrast to classical nonlinear materials.

Inspired by these prospects, many different designs were investigated. Second-[10−14] and third-harmonic generation,[15,16] four-wave mixing,[17−19] and multiphoton photoluminescence[20,21] from single nanostructures[22−24] as well as from arrays of particles[25−28] have been studied in great detail. It soon became apparent that the measured signals and conversion efficiencies were surprisingly large, in particular when taking the nanoscale volume of the structures into account. While many aspects of the generation processes are still not fully understood, quite a few details of the working principles could be unraveled: Third-harmonic (TH) signals seem to be generated predominantly in the volume of the plasmonic nanostructures.[29,30] Second-harmonic processes seem to be more sensitive to surfaces, interfaces, and structural defects of the nanosystems,[31−35] yet, they are still related to the plasmonic material itself. For the actual nonlinear conversion two distinct processes have to be considered. First, the enhanced electric near-fields associated with the plasmon resonances are driving the local nonlinear conversion. Second, the conversion itself takes places inside the plasmonic material; that is, it is ultimately related to its bulk nonlinearity. Assuming a realistic

Received: January 18, 2018
Published: March 23, 2018

DOI: 10.1021/acsphotonics.8b00079
ACS Photonics 2018, 5, 1863−1870

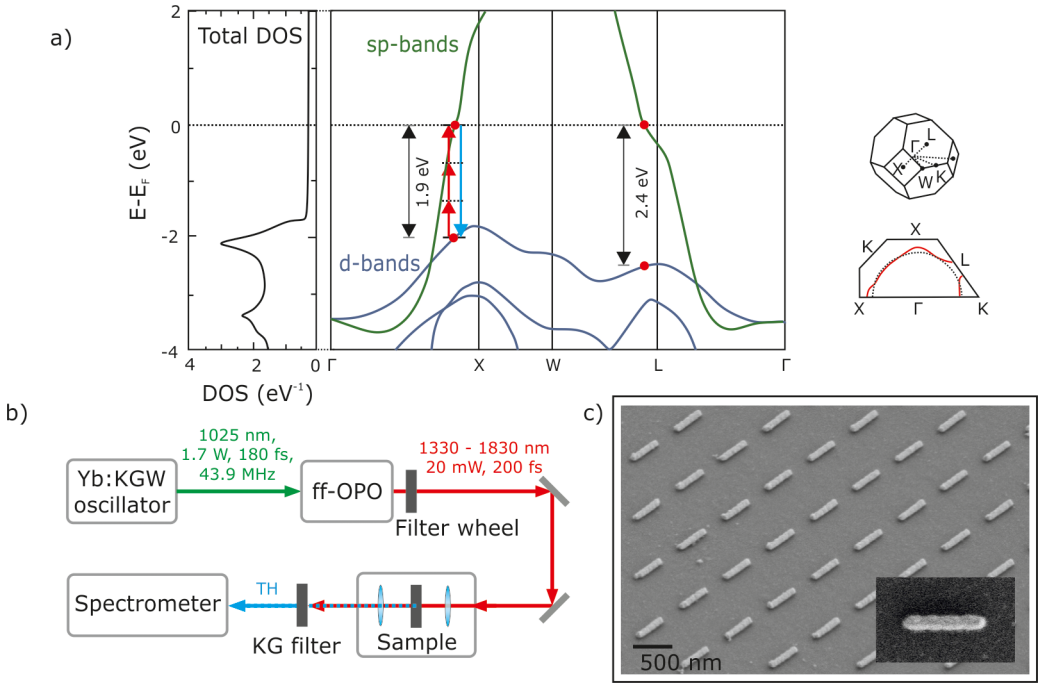

Figure 1. (a) Sketch of the band structure of gold (middle), density of states (DOS) (left), and the crystal structure (with crystal directions) and Fermi surface (right). The optical properties of gold are mainly determined by the partially filled 6sp-bands. Interband transitions from the 5d- to the 6sp-band setting in at 1.9 and 2.4 eV modify the behavior (red dots). These resonant transitions can enhance a third-harmonic process as soon as three-photon transitions (red arrows) from the d-band to the sp-band become possible. The resonant emission of the TH photon is indicated by the blue arrow. Resonant states are visualized by solid lines; virtual levels by dashed lines. Figure is based on refs 44 and 45. (b) Sketch of the experimental setup, utilizing a broadband-tunable fiber-feedback optical parametric oscillator. For details see the main text. (c) Overview scanning electron microscopy (SEM) image of an exemplary antenna array used for third-harmonic spectroscopy. The inset shows a single antenna of 380 nm length.

local field enhancement on the order of 10−50,[36] the observed nonlinear signals are in fact pointing to a large bulk nonlinearity. This intrinsic material third-order susceptibility ($\chi^{(3)}$) of gold, which is the most commonly used plasmonic material to date, therefore seems to significantly surpass common bulk nonlinear materials,[19,37] which appears counterintuitive. The scope of this work is hence to investigate the nature of the resonant enhancement of the gold nonlinearity.

While all the structural aspects have been studied in great detail,[38,39] this material aspect has often been overlooked despite the fact that it offers an additional degree of freedom in design. One possible explanation for the surprisingly large absolute values of the gold third-order susceptibility is related to *resonant* material nonlinearities. It is known from crystal nonlinear optics that absorptive material transitions at the fundamental or higher harmonic of the incident laser intensity can significantly enhance the generation process,[40] driving the nonlinear susceptibility into resonance. This holds true even if the material becomes basically opaque at the respective wavelength. It is therefore compelling to suspect resonant gold interband transitions from the 5s- to the 6sp-band of gold to be involved in the nonlinear conversion process that sets in between 500 and 600 nm. Previous works indeed hypothesized that d-band transitions could play an important role,[32,41] yet only little experimental effort has been undertaken to quantitatively analyze their exact role.[42,43]

To unambiguously determine the exact nonlinear contribution of interband transitions, it is necessary to measure the quantitative dispersion of the gold third-order susceptibility. As the interband transitions are in fact resonant ones, the absolute $\chi^{(3)}$ values will also be strongly dispersive. There are two possibilities to account for this issue. On one hand, one can investigate plasmonic systems off-resonant leading to low TH signals, as in the case of the complex nanoparticle-overfilm geometry studied by Hajisalem et al.[43] On the other hand, employing plasmonic resonances is beneficial due to the enhanced response of the bare gold nonlinearity, delivering a good signal-to-noise ratio, while adding additional dispersion due to the spectrally dependent local field enhancement. In order to understand the comparably strong nonlinear signals in these plasmonic systems, it is therefore crucial to disentangle the contributions of the plasmonic resonances and the material nonlinearity, ideally in a direct fashion via precise knowledge of the linear plasmonic response. We solve this issue by combining both approaches independently, measuring a resonantly excited plasmonic system while using a bare gold film as an independent reference measurement.

To fully extract the involvement of d-band transitions, it is indispensable to measure the nonlinear conversion in spectral regions in which it is energetically possible to involve an interband transition at the harmonic wavelength and in regions in which such transitions are energetically not excitable. Additionally, a broadly tunable light source with high repetition rate, high stability, spectral and pulse quality, and close to Fourier-bandwidth-limited pulses is required that spans the wavelength region of interest between 1300 and 1800 nm. Moreover, it is absolutely crucial to employ a reliable normalization scheme to correct for seemingly minute changes in laser power, focus size, and pulse duration. In this way we eliminate any artifacts leading to high signal-to-noise ratio measurements.[42,43]

DOI: 10.1021/acsphotonics.8b00079
ACS Photonics 2018, 5, 1863−1870

We utilize well-designed and spectrally fully characterized resonant plasmonic rod nanoantennas in our experiments, as they offer a high quality factor (higher than, for example, discs) and feature just a single well-pronounced plasmonic mode in the spectral region of interest for excitation along the antenna axis, which makes them the simplest plasmonic system at hand. Additionally, the simple dipolar resonance of the rod-shaped antennas can be modeled by the well-known anharmonic oscillator model in order to obtain *independent a priori predictions* about the radiated TH signals, which is not possible for the gold nanoparticle-over-gold film geometry.[43] Modeling the plasmon mode of the nanoantennas based on their experimentally obtained linear optical properties thus allows us to extract the quantitative dispersion of the third-order gold nonlinearity over a broad spectral region without the need of using an indirect reference method such as multiphoton photoluminescence.[42] We perform spectroscopic measurements in transmission in the near-infrared (near-IR) between 1330 and 1830 nm wavelength, corresponding to TH radiated between 443 and 610 nm wavelength. We find that the radiated TH signals do indeed significantly increase at the onset of interband transitions, that is, as soon as the TH becomes resonant with interband transitions, rendering the nonlinear third-order susceptibility of gold highly wavelength-dependent in the near-IR wavelength range. This strong dispersion of the third-order nonlinearity of gold convincingly demonstrates the role of d-band transitions in the large absolute values of the third-order gold nonlinearity.

The optical and electronic properties of gold are mainly determined by a partially filled 6sp-band, as shown in the gold band structure diagram in Figure 1a. The optical properties arising from these electrons are excellently described by a Drude model for a free-electron gas. The Drude model works well for energies below about 1.9 eV (652 nm) at which interband transitions near the X-point from the fully filled 5d-band to the 6sp-band start to set in (indicated by two red dots in Figure 1a).[44] Another modification arises from the additional interband transition onset at about 2.4 eV (517 nm) near the L-point (again indicated by two red dots). This behavior can be phenomenologically described by a Drude−Lorentz model, which takes this additional absorption of photons by interband transitions into account. It should be noted that the interband contributions do not set in in a step-like fashion but gradually increase, starting at the first onset at 1.9 eV, overtaking the Drude absorption at about 2 eV and only strongly increasing at the second onset at 2.4 eV (for further details see Figure S1 in the Supporting Information). These interband transitions are also responsible for the yellowish appearance of gold as mainly the green and blue parts of the visible spectrum are absorbed.

The interband transitions from the 5d- to the 6sp-bands are resonant absorptive transitions. These transitions can therefore resonantly enhance a nonlinear conversion process. This phenomenon is illustrated with red and blue arrows for the transition near the X-point for energies right at the transition onset at 1.9 eV. The energy of the incident fundamental photons (red arrows) is exactly one-third of the transition energy (1.9 eV). By absorbing three fundamental photons at frequency ω, an electron can be excited from the 5d-band into the 6sp-bands. This process is highly efficient due to the large density of states (DOS) associated with the 5d-band (illustrated in the left panel of Figure 1a).[44] The nonlinear susceptibility, which depends on the optical properties of the material at the fundamental and the higher harmonic of the incident light, is therefore resonantly enhanced, boosting the conversion efficiency. It is important to note that such an excitation is possible for all TH processes at TH energies above the transition onset at 1.9 eV. The same general process can be envisioned at the interband transition onset near the L-point for energies around 2.4 eV. Both transitions are thus expected to substantially modify the nonlinear conversion and thus influence the third-order gold susceptibility. However, due to the fact that two distinct transition onsets at different energies are involved and due to the comparably small DOS in the 6sp-bands, we do not expect an abrupt step-like transition between the resonant and off-resonant nonlinearity regimes, but rather a gradual transition. This fact additionally underlines the importance of a broadband-tunable light source to cover a large enough spectral region.

Our experimental setup is sketched in Figure 1b. A femtosecond Yb:KGW solid-state oscillator at 44 MHz repetition rate[46] is used to pump a fiber-feedback optical parametric oscillator (ff-OPO).[47−49] The ff-OPO signal wavelength tuning range spans from about 1330 to 1830 nm with a constant pulse duration of about 200 fs. In Figure S2 of the Supporting Information we show selected representative fundamental laser spectra. The nearly Fourier-bandwidth-limited pulses exhibit a Gaussian shape with constant spectral width over the entire tuning range. The output power level is set to a constant value of 20 mW for all wavelengths using a neutral density filter wheel. This value was found as a trade-off between TH signal strength and possible sample damage. The ff-OPO signal beam is focused onto the nanoantenna arrays with the electric field polarized parallel to the long axis of the antennas to excite the plasmonic resonance most effectively. The generated TH signals in the forward direction are collected using a second lens and separated from the remaining ff-OPO signal and are finally coupled into a grating spectrometer with attached charge-coupled device (CCD) for spectrally resolved detection. In general, the radiated TH signals are determined by the symmetry of the system and thus the nonvanishing tensor components describing the entire system. Experimentally, we find the polarization of the generated TH to be along the antenna long axis, which is consistent with previous reports.[16,50] For further information on our measurement setup, see the Supporting Information.

The nanoantenna arrays are fabricated using standard electron beam lithography on an ultraviolet (UV) transparent glass substrate. The different arrays have a size of 100 × 100 μm^2. The antennas consist of 2 nm chromium and 60 nm gold. Their lengths are tuned in steps of 20 nm from 380 to 520 nm, while their width is kept constant at 60 nm. Due to the very large spectral tuning range, special precautions have to be taken regarding antenna periodicity. In order to avoid both near-field coupling between the single antennas and Rayleigh anomalies, the periodicity is adjusted for every antenna length. In our experiment the distance between the long axis of the antennas is kept constant at 300 nm for all arrays, resulting in a periodicity in the x- and y-direction of length + 300 nm. A representative tilted overview scanning electron microscope (SEM) image of an antenna array is shown in Figure 1c. The inset depicts a close-up of a single antenna. Additional fabrication details can be found in the Supporting Information.

Figure 2a depicts the linear extinction (1-transmittance) spectra of our investigated antenna arrays, measured utilizing a Fourier-transform infrared spectrometer (FTIR) Bruker Vertex, equipped with a Hyperion microscope. The resonance

DOI: 10.1021/acsphotonics.8b00079
ACS Photonics 2018, 5, 1863−1870

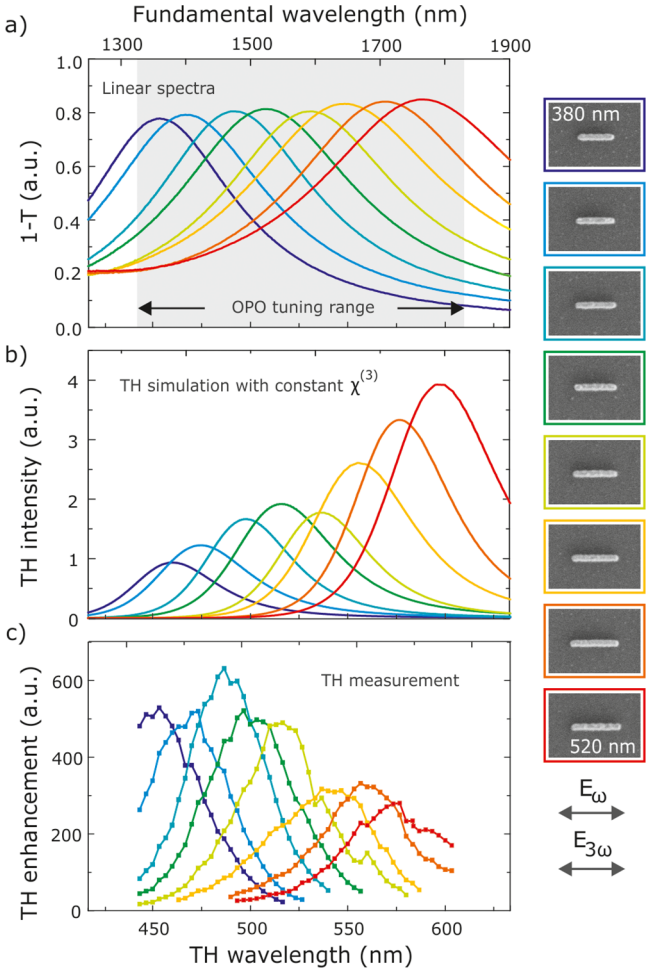

Figure 2. (a) Linear plasmon resonances of eight gold nanoantenna arrays with varying length (380 to 520 nm in 20 nm steps, exemplary SEM images as legend). The gray-shaded area indicates the tuning range of the employed optical parametric oscillator. (b) Simulation results of the third-harmonic enhancement curves based on an anharmonic oscillator model assuming a constant microscopic gold nonlinearity $\chi^{(3)}$. (c) Measured TH enhancement factor (compared to the TH of the bare UV-fused silica substrate) as a function of the fundamental wavelength for eight different antenna arrays. In stark contrast to (b) a decrease in the maximum TH enhancement is observed when shifting the fundamental resonance wavelength to longer wavelengths. This observation suggests a wavelength-dependent gold nonlinearity that decreases for increasing wavelength.

wavelength of the eight different antenna arrays spans the entire ff-OPO tuning range between roughly 1300 and 1850 nm (gray-shaded area) and thus also the suspected transition region with the onset of interband transitions at the TH wavelength at around 550 nm (corresponding to a 1650 nm fundamental wavelength). The linear spectra for incident light polarized along the antenna short axis are shown in Figure S3 in the Supporting Information and exhibit a weakly modulated plasmonic mode at around 550 nm for all antenna lengths. Previous reports have shown that the presence of a resonance at the higher harmonic wavelength can influence the nonlinear generation process if the radiated higher harmonic signal is polarized along the polarization direction of this mode.[51,52] In our case the TH signal is radiated along the antenna long axis, which renders the influence of the short axis mode minor at best. Adjusting the array period, as discussed above, results in very similar linear properties. Importantly, the quality factor of all antenna arrays is nearly the same, as is the overall oscillator strength,[53] which is crucial in nonlinear plasmonic experiments, as is the constant pulse duration and the incident power level.

As a first step, we predict the nonlinear optical response of our different antenna arrays using a well-established anharmonic oscillator model.[29,30,53,54] A damped, driven harmonic oscillator with a small cubic perturbation b is used to calculate the radiated TH signals:

$$\ddot{x} + 2\gamma\dot{x} + {\omega_0}^2 x + bx^3 = -\frac{e}{m}E_x(t)$$

Here, γ denotes the damping constant, ω_0 the plasmon resonance frequency, and e and m the charge and mass of an electron, respectively. It is important to note that the perturbation parameter b describes the nonlinearity of the systems and is thus ultimately related to the nonlinear susceptibility $\chi^{(3)}$ of gold, which is most generally described by a tensor of rank 4. This tensorial description takes all local polarization dependences into account and also incorporates the polarization dependences that might be present in the interaction with d-band states. However, previous work has shown that a scalar description of the third-order gold nonlinearity is fully sufficient. This can most likely be explained on one hand by the local near-field distribution which strongly deviates from the far-field polarization state due to the presence of the plasmonic resonance and, on the other hand, by the fact that the antenna is composed of individual gold grains, which have a size of roughly 25 nm in each direction, leading effectively to a pseudoamorphous state.

To perform the simulation for all antenna arrays, the plasmon resonances are fitted using the following expression for the linear extinction:

$$\alpha(\omega) = \frac{e^2 n}{\varepsilon_0 cm}\frac{\gamma\omega^2}{(\omega^2 - {\omega_0}^2)^2 + 4\gamma^2\omega^2}$$

From this fit we extract γ ,ω_0, and the factor$A = \frac{e^2 n}{\varepsilon_0 cm}$. Two aspects are important here: The factor A/n is in fact the oscillator strength of our antennas and is linked to the surface area of the resonance curves, thus being ultimately related to the number of quasi-free electrons in the system. The factor n is the oscillator density in our system. We thus find that the change in antenna density, which results from the different periodicities, is in fact fully described by the model. It is important to note that imperfections of the fabricated antennas as well as the graininess are naturally included in our model due to their influence on the plasmon resonance, which manifest themselves, for example, in the line width of the experimentally measured resonance.

Using these fitting parameters of the plasmon resonance our model can predict the spectral position, the width, and the amplitude of the TH enhancement curves for our different antenna arrays. These simulations, utilizing a spectrally constant nonlinearity parameter b, are plotted in Figure 2b. The predicted maximum TH enhancement increases significantly with longer plasmon resonance wavelength.

Next, we perform the TH measurements for all eight gold nanoantenna arrays. In order to ensure resonant excitation, we perform spectrally resolved nonlinear spectroscopy on the different nanoantenna arrays. This measurement thus delivers the full TH enhancement curves for all antenna arrays, which are directly comparable to the simulated ones in Figure 2b. The

DOI: 10.1021/acsphotonics.8b00079
ACS Photonics 2018, 5, 1863−1870

ff-OPO signal is swept in steps of 10 nm over each plasmon resonance, and the generated TH spectrum is measured for each fundamental wavelength point. Exemplary TH spectra are shown in Figure S4 in the Supporting Information. Within the measurements' accuracy we do not observe multiphoton photoluminescence. This allows us to spectrally integrate the TH spectra without additional modeling or correction in order to obtain a scalar value describing the overall TH enhancement at each measured wavelength point. These values are then normalized to the TH radiated by the surface of a 5 mm thick UV-fused silica substrate (avoiding interference of front and back TH) to eliminate all possible wavelength dependences of the setup (filters, detector, fundamental intensity, etc.).

The resulting TH enhancement curves as a function of wavelength are shown in Figure 2c using the same color code as in panels a and b. In stark contrast to the simulation shown in panel b we observe a strong decrease of the maximum TH enhancement for longer wavelength. The conversion efficiency is therefore larger for shorter wavelengths despite similar oscillator properties. This behavior clearly suggests that the assumption of a constant nonlinearity parameter b is in fact not justified. The nonlinearity seems to decrease for longer wavelength. Additionally, we observe an increasing spectral blue shift between the point of largest TH conversion efficiency and the linear resonance position of the antenna arrays. This observation also suggests a strongly wavelength-dependent nonlinearity that is larger for shorter wavelengths, which effectively blue-shifts the TH enhancement curves.

To further elucidate the observed behavior, we require an experimental measure of the intrinsic third-order gold nonlinearity and thus perform TH spectroscopy of a 20 nm thick gold film. We measured the TH radiated from the film over the entire tuning range in steps of 10 nm and normalized it to the TH from the UV-fused silica substrate. As we assume the gold nonlinearity to change due to the onset of strong absorption at the TH wavelength, we need to correct the measured TH signals for the intrinsic absorption of the gold film. In accordance with the literature, we assume the TH to be generated at the gold interfaces.[55,56] As the fundamental intensity is significantly attenuated by the gold film (skin depth 23 nm at 1500 nm wavelength),[57] we assume that all radiated TH is generated solely at the front interface. Thus, the absorption of the gold film at the TH wavelength needs to be taken into account. The absorption spectrum of the semi-infinite gold film in the TH wavelength range has been calculated employing an analytical model using experimentally obtained data for the dielectric function of gold.[58] The measured relative TH intensity is shown in Figure 3a. The TH intensity is about 5-fold larger in the shorter wavelength range when compared to the long-wavelength end. We are thus observing a strong wavelength dependence of the microscopic gold nonlinearity. The increase to shorter wavelength is gradual and not stepwise, as is expected from the gold band structure diagram and the related density of states (see above). Between 1800 and 1700 nm only a slight increase in the TH signal is observed; however, at around 1600 nm the signal starts to rise strongly. This behavior underpins the involvement of the resonant interband transitions, which indeed both start to contribute significantly at around 517 nm TH wavelength and thus a fundamental wavelength of 1551 nm. The measured values start to flatten out at large nonlinear efficiency around 1400 nm, where the TH wavelength is well inside the strong interband transition region.

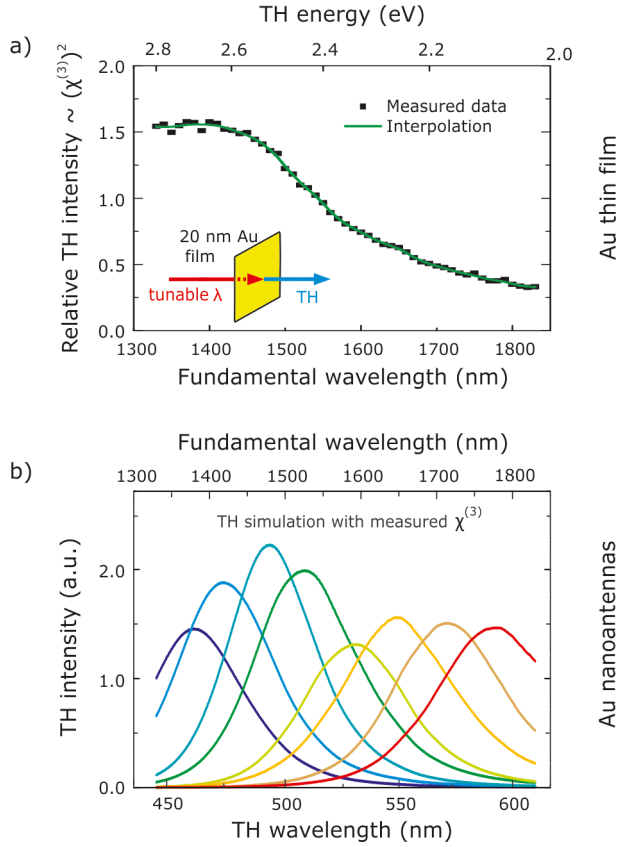

Figure 3. (a) Measured wavelength-dependent third-order microscopic nonlinearity of a 20 nm thick gold film (referenced to a thick UV-fused silica substrate). (b) Simulation of the TH enhancement curves for all eight antenna arrays based on the anharmonic oscillator model, taking the wavelength-dependent microscopic nonlinearity $\chi^{(3)}(\omega)$ of gold from (a) into account. These TH spectra exhibit similar behavior to the measurement results in Figure 2c.

To further strengthen this interpretation, we modify our anharmonic oscillator model to include the measured wavelength dependence of the intrinsic gold nonlinearity, as shown in Figure 3a. The nonlinearity parameter b of our model is proportional to the square of the gold third-order susceptibility $\chi^{(3)}(\omega)$, as is the measured relative TH intensity of the gold film, which is then used to modify the previous simulation results. If our interpretation is correct, the model needs to be able to describe the two observed features of the experimental spectra in Figure 2b, namely, the decrease in TH conversion for longer wavelength and the observed spectral blue shift. Figure 3b plots the results of the modified anharmonic oscillator modeling. We indeed observe the same decrease of the maximum TH enhancement as in the experiment. Overall, there is excellent agreement in the relative TH enhancements of the different antenna arrays. In the simulation we now also observe the spectral blue shift of the peak TH conversion efficiency.

Additional details of our measurement and simulation are discussed in Figure 4, where we show the linear response and the measured and the simulated TH enhancement curves for three different antenna arrays in one diagram each. The simulation now takes the measured wavelength-dependent dispersion of the gold nonlinearity $\chi^{(3)}(\omega)$ from Figure 3a into account.

DOI: 10.1021/acsphotonics.8b00079
ACS Photonics 2018, 5, 1863−1870

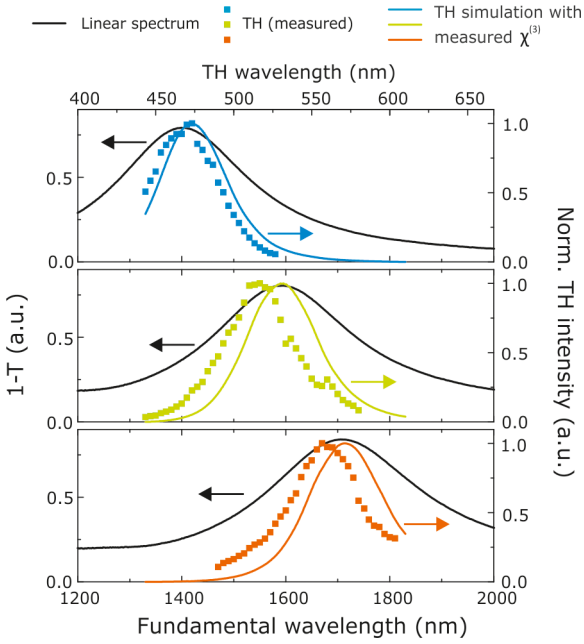

Figure 4. Linear extinction (1-transmittance) spectra of the plasmon resonances of three different antenna arrays (black lines) with the corresponding measured normalized TH enhancement curves (colored dots). The anharmonic oscillator simulation results including the measured wavelength-dependent dispersion of the gold nonlinearity $\chi^{(3)}(\omega)$ are shown as solid colored lines and show a slight red shift compared to the measurement. Overall, simulation and measurement agree well.

Let us first compare the linear spectra with the simulated TH enhancement curves: The maximum TH enhancement is normally observed red-shifted with respect to the far-field extinction spectrum.[16] As the radiated TH signal is ultimately generated by the intrinsic gold nonlinearity driven by the local field enhancement, the maximum TH is expected at the wavelength where the maximal near-field strength occurs. Due to the intrinsic damping of the plasmon, this maximum near-field occurs red-shifted with respect to the far-field response, as has been reported earlier.[59−61] For the shortest wavelength antenna array we indeed observe a red shift. For the two longer wavelength antenna arrays, this red shift diminishes and the modeled maximum TH enhancement coincides now with the linear far-field extinction maximum. This behavior is caused by the wavelength-depended gold nonlinearity, which increases for shorter wavelength and thus counteracts the described red shift in the case of the two longer resonance wavelength antenna arrays. For the shorter wavelength resonance array, the gold nonlinearity is nearly spectrally flat and thus does not shift the curve (cf. Figure 3a).

We now compare the modeled TH enhancement curves with the measured one. We observe a clear spectral shift between measurements and simulation. This at first sight surprising observation can in fact be straightforwardly explained: It is well known that the exact spectral position of a plasmonic resonance depends on the excitation. In order to obtain broadband linear spectra in the IR, one requires the use of an FTIR setup, as discussed above. Here, the angled illumination geometry is quite different from normal incidence plane wave excitation, which is the case for laser illumination. We thus in fact expect a spectral shift between the two spectra. Figure S5 in the Supporting Information indeed proves that the linear resonance measured with the FTIR setup is red-shifted with respect to the same resonance measured with the ff-OPO as white light source. The observed shift between the simulated TH enhancement and the measured one is therefore inconsequential. Hence, when disregarding this shift, we see good agreement between model and measurement in terms of width and shape of the TH enhancement curves, which once more underlines the validity of our findings. For a direct comparison of simulation with and without the wavelength-dependent nonlinearity and measurement, refer to Figure S6 in the Supporting Information.

In conclusion, we unambiguously demonstrated that the microscopic third-order nonlinearity of gold is strongly influenced by interband transitions from the 5d- to the 6sp-bands. The gold nonlinearity is hence a resonant nonlinearity, explaining in part the large observed conversion efficiencies of gold nanoantennas. This resonant material nonlinearity is hence another design parameter that can be used to tailor and manipulate the nonlinear response of plasmonic nanostructures. It is interesting to note that resonant enhancement is often accompanied by unwanted material losses. When enhancing the fundamental frequency component, this effect is strongest and less severe while also generally less efficient when enhancing the higher harmonic component. Here, the resonant enhancement is in fact an intrinsic property of the material and cannot be manipulated, but nevertheless leads to a significant enhancement of the system's nonlinearity. Our work thus motivates the investigation of other plasmonic materials, particularly metals such as silver, copper, and aluminum with different band structures, which should allow for very efficient nonlinear conversion into the blue and UV spectral region. Furthermore, more complex systems, e.g., dimers, offer additional degrees of freedom and are thus highly intriguing for future studies.

■ ASSOCIATED CONTENT

Supporting Information

The Supporting Information is available free of charge on the ACS Publications website at DOI: 10.1021/acsphotonics.8b00079.

Figures of dielectric function of gold, signal spectra of the ff-OPO, linear plasmon resonance of the antenna short axis, single TH spectra showing no detectable multiphoton photoluminescence and TH spectra of a gold antenna array, dependence of the plasmon resonance on different light sources, and comparison of measured and simulated spectra; detailed description of the experimental setup and sample fabrication (PDF)

■ AUTHOR INFORMATION

Corresponding Author

*E-mail: j.krauth@pi4.uni-stuttgart.de.

ORCID

Joachim Krauth: 0000-0001-9683-762X

Notes

The authors declare no competing financial interest.

■ ACKNOWLEDGMENTS

We acknowledge financial support from the European Research Council (ERC Advanced Grant Complexplas), Bundesministerium für Bildung and Forschung, Deutsche Forschungsgemein-

DOI: 10.1021/acsphotonics.8b00079
ACS Photonics 2018, 5, 1863−1870

schaft (SPP1839 and SPP1391), and Baden-Württemberg Stiftung. We thank Bernd Metzger and Martin Schäferling for discussions and Tobias Steinle for technical support.

REFERENCES

(1) Boyd, R. W. *Nonlinear Optics*, 3; Academic: Rochester, NY, 2007.
(2) Sutherland, R. L. *Handbook of Nonlinear Optics*; Marcel Dekker: New York, 2003; Vol. 36.
(3) Voelkmann, C.; Reichelt, M.; Meier, T.; Koch, S. W.; Höfer, U. Five-Wave-Mixing Spectroscopy of Ultrafast Electron Dynamics at a Si(001) Surface. *Phys. Rev. Lett.* **2004**, *92*, 127405.
(4) Kravtsov, V.; Ulbricht, R.; Atkin, J. M.; Raschke, M. B. Plasmonic Nanofocused Four-Wave Mixing for Femtosecond near-Field Imaging. *Nat. Nanotechnol.* **2016**, *11*, 459−464.
(5) Kauranen, M.; Zayats, A. V. Nonlinear Plasmonics. *Nat. Photonics* **2012**, *12*, 737−748.
(6) Hasan, S. B.; Lederer, F.; Rockstuhl, C. Nonlinear Plasmonic Antennas. *Mater. Today* **2014**, *17*, 478−485.
(7) Bouhelier, A.; Beversluis, M.; Hartschuh, A.; Novotny, L. Near-Field Second-Harmonic Generation Induced by Local Field Enhancement. *Phys. Rev. Lett.* **2003**, *90*, 13903.
(8) Novotny, L.; Van Hulst, N. Antennas for Light. *Nat. Photonics* **2011**, *5*, 83−90.
(9) Halas, N. J.; Lal, S.; Chang, W. S.; Link, S.; Nordlander, P. Plasmons in Strongly Coupled Metallic Nanostructures. *Chem. Rev.* **2011**, *111*, 3913−3961.
(10) Niesler, F. B. P.; Feth, N.; Linden, S.; Wegener, M. Second-Harmonic Optical Spectroscopy on Split-Ring-Resonator Arrays. *Opt. Lett.* **2011**, *36*, 1533−1535.
(11) Klein, M. W.; Enkrich, C.; Wegener, M.; Linden, S. Second-Harmonic Generation from Magnetic Metamaterials. *Science* **2006**, *313*, 502−504.
(12) Linden, S.; Niesler, F. B. P.; Förstner, J.; Grynko, Y.; Meier, T.; Wegener, M. Collective Effects in Second-Harmonic Generation from Split-Ring-Resonator Arrays. *Phys. Rev. Lett.* **2012**, *109*, 15502.
(13) Celebrano, M.; Wu, X.; Baselli, M.; Großmann, S.; Biagioni, P.; Locatelli, A.; De Angelis, C.; Cerullo, G.; Osellame, R.; Hecht, B.; et al. Mode Matching in Multiresonant Plasmonic Nanoantennas for Enhanced Second Harmonic Generation. *Nat. Nanotechnol.* **2015**, *10*, 412−417.
(14) Aouani, H.; Navarro-Cia, M.; Rahmani, M.; Sidiropoulos, T. P. H. H.; Hong, M.; Oulton, R. F.; Maier, S. A. Multiresonant Broadband Optical Antennas As Efficient Tunable Nanosources of Second Harmonic Light. *Nano Lett.* **2012**, *12*, 4997−5002.
(15) Lippitz, M.; van Dijk, M. A.; Orrit, M. Third-Harmonic Generation from Single Gold Nanoparticles. *Nano Lett.* **2005**, *5*, 799−802.
(16) Metzger, B.; Hentschel, M.; Lippitz, M.; Giessen, H. Third-Harmonic Spectroscopy and Modeling of the Nonlinear Response of Plasmonic Nanoantennas. *Opt. Lett.* **2012**, *37*, 4741−4743.
(17) Danckwerts, M.; Novotny, L. Optical Frequency Mixing at Coupled Gold Nanoparticles. *Phys. Rev. Lett.* **2007**, *98*, 26104.
(18) Palomba, S.; Danckwerts, M.; Novotny, L. Nonlinear Plasmonics with Gold Nanoparticle Antennas. *J. Opt. A: Pure Appl. Opt.* **2009**, *11*, 114030.
(19) Zhang, Y.; Wen, F.; Zhen, Y.-R.; Nordlander, P.; Halas, N. J. Coherent Fano Resonances in a Plasmonic Nanocluster Enhance Optical Four-Wave Mixing. *Proc. Natl. Acad. Sci. U. S. A.* **2013**, *110*, 9215−9219.
(20) Biagioni, P.; Brida, D.; Huang, J. S.; Kern, J.; Duò, L.; Hecht, B.; Finazzi, M.; Cerullo, G. Dynamics of Four-Photon Photoluminescence in Gold Nanoantennas. *Nano Lett.* **2012**, *12*, 2941−2947.
(21) Knittel, V.; Fischer, M. P.; De Roo, T.; Mecking, S.; Leitenstorfer, A.; Brida, D. Nonlinear Photoluminescence Spectrum of Single Gold Nanostructures. *ACS Nano* **2015**, *9*, 894−900.
(22) Zhang, Y.; Grady, N. K.; Ayala-Orozco, C.; Halas, N. J. Three-Dimensional Nanostructures as Highly Efficient Generators of Second Harmonic Light. *Nano Lett.* **2011**, *11*, 5519−5523.
(23) Hanke, T.; Cesar, J.; Knittel, V.; Trügler, A.; Hohenester, U.; Leitenstorfer, A.; Bratschitsch, R. Tailoring Spatiotemporal Light Confinement in Single Plasmonic Nanoantennas. *Nano Lett.* **2012**, *12*, 992−996.
(24) Harutyunyan, H.; Volpe, G.; Quidant, R.; Novotny, L. Enhancing the Nonlinear Optical Response Using Multifrequency Gold-Nanowire Antennas. *Phys. Rev. Lett.* **2012**, *108*, 217403.
(25) Feth, N.; Linden, S.; Klein, M. W.; Decker, M.; Niesler, F. B. P.; Zeng, Y.; Hoyer, W.; Liu, J.; Koch, S. W.; Moloney, J. V.; et al. Second-Harmonic Generation from Complementary Split-Ring Resonators. *Opt. Lett.* **2008**, *33*, 1975−1977.
(26) Ko, K. D.; Kumar, A.; Fung, K. H.; Ambekar, R.; Liu, G. L.; Fang, N. X.; Toussaint, K. C. Nonlinear Optical Response from Arrays of Au Bowtie Nanoantennas. *Nano Lett.* **2011**, *11*, 61−65.
(27) Metzger, B.; Hentschel, M.; Giessen, H. Probing the Near-Field of Second-Harmonic Light around Plasmonic Nanoantennas. *Nano Lett.* **2017**, *17*, 1931−1937.
(28) Linnenbank, H.; Grynko, Y.; Förstner, J.; Linden, S. Second Harmonic Generation Spectroscopy on Hybrid Plasmonic/dielectric Nanoantennas. *Light: Sci. Appl.* **2016**, *5*, e16013.
(29) Wolf, D.; Schumacher, T.; Lippitz, M. Shaping the Nonlinear near Field. *Nat. Commun.* **2016**, *7*, 10361.
(30) Metzger, B.; Schumacher, T.; Hentschel, M.; Lippitz, M.; Giessen, H. Third Harmonic Mechanism in Complex Plasmonic Fano Structures. *ACS Photonics* **2014**, *1*, 471−476.
(31) Zayats, A. V.; Kalkbrenner, T.; Sandoghdar, V.; Mlynek, J. Second-Harmonic Generation from Individual Surface Defects under Local Excitation. *Phys. Rev. B: Condens. Matter Mater. Phys.* **2000**, *61*, 4545−4548.
(32) Butet, J.; Brevet, P.-F.; Martin, O. J. F.; Pierre-Francois Brevet; Martin, O. J. F. . Optical Second Harmonic Generation in Plasmonic Nanostructures: From Fundamental Principles to Advanced Applications. *ACS Nano* **2015**, *9*, 10545−10562.
(33) Butet, J.; Thyagarajan, K.; Martin, O. J. F. Ultrasensitive Optical Shape Characterization of Gold Nanoantennas. *Nano Lett.* **2013**, *13*, 1787−1792.
(34) Canfield, B.; Kujala, S.; Jefimovs, K.; Turunen, J.; Kauranen, M. Linear and Nonlinear Optical Responses Influenced by Broken Symmetry in an Array of Gold Nanoparticles. *Opt. Express* **2004**, *12*, 5418−5423.
(35) Czaplicki, R.; Zdanowicz, M.; Koskinen, K.; Laukkanen, J.; Kuittinen, M.; Kauranen, M. Dipole Limit in Second-Harmonic Generation from Arrays of Gold Nanoparticles. *Opt. Express* **2011**, *19*, 26866−26871.
(36) Fischer, H.; F Martin, O. J. Engineering the Optical Response of Plasmonic Nanoantennas. *Opt. Express* **2008**, *16*, 9144−9154.
(37) Renger, J.; Quidant, R.; Van Hulst, N.; Novotny, L. Surface-Enhanced Nonlinear Four-Wave Mixing. *Phys. Rev. Lett.* **2010**, *104*, 46803.
(38) Valev, V. K.; Silhanek, A. V.; Verellen, N.; Gillijns, W.; Van Dorpe, P.; Aktsipetrov, O. A.; Vandenbosch, G. A. E. E.; Moshchalkov, V. V.; Verbiest, T. Asymmetric Optical Second-Harmonic Generation from Chiral G-Shaped Gold Nanostructures. *Phys. Rev. Lett.* **2010**, *104*, 127401.
(39) O'Brien, K.; Suchowski, H.; Rho, J.; Salandrino, A.; Kante, B.; Yin, X.; Zhang, X. Predicting Nonlinear Properties of Metamaterials from the Linear Response. *Nat. Mater.* **2015**, *14*, 379−383.
(40) Fiebig, M.; Pavlov, V. V.; Pisarev, R. V. Second-Harmonic Generation as a Tool for Studying Electronic and Magnetic Structures of Crystals: Review. *J. Opt. Soc. Am. B* **2005**, *22*, 96−118.
(41) Hanke, T.; Krauss, G.; Träutlein, D.; Wild, B.; Bratschitsch, R.; Leitenstorfer, A. Efficient Nonlinear Light Emission of Single Gold Optical Antennas Driven by Few-Cycle near-Infrared Pulses. *Phys. Rev. Lett.* **2009**, *103*, 257404.
(42) Knittel, V.; Fischer, M. P.; Vennekel, M.; Rybka, T.; Leitenstorfer, A.; Brida, D. Dispersion of the Nonlinear Susceptibility in Gold Nanoantennas. *Phys. Rev. B: Condens. Matter Mater. Phys.* **2017**, *96*, 125428.

DOI: 10.1021/acsphotonics.8b00079
ACS Photonics 2018, 5, 1863−1870

(43) Hajisalem, G.; Hore, D. K.; Gordon, R. Interband Transition Enhanced Third Harmonic Generation from Nanoplasmonic Gold. *Opt. Mater. Express* **2015**, *5*, 2217−2224.
(44) Raschke, M. B.; Berweger, S.; Atkin, J. M.; Shahbazyan, T. V.; Stockman, M. I. Ultrafast and Nonlinear Plasmon Dynamics. In *Plasmonics: Theory and Applications*; Springer: Dordrecht, 2013; pp 237−281.
(45) Ladstädter, F.; Hohenester, U.; Puschnig, P.; Ambrosch-Draxl, C. First-Principles Calculation of Hot-Electron Scattering in Metals. *Phys. Rev. B: Condens. Matter Mater. Phys.* **2004**, *70*, 235125.
(46) Metzger, B.; Steinmann, A.; Giessen, H. High-Power Widely Tunable Sub-20fs Gaussian Laser Pulses for Ultrafast Nonlinear Spectroscopy. *Opt. Express* **2011**, *19*, 24354−24360.
(47) Südmeyer, T.; Aus der Au, J.; Paschotta, R.; Keller, U. Femtosecond Fiber-Feedback Optical Parametric Oscillator. *Opt. Lett.* **2001**, *26*, 304−306.
(48) Mörz, F.; Steinle, T.; Steinmann, A.; Giessen, H. Multi-Watt Femtosecond Optical Parametric Master Oscillator Power Amplifier at 43 MHz. *Opt. Express* **2015**, *23*, 23960−23967.
(49) Steinle, T.; Neubrech, F.; Steinmann, A.; Yin, X.; Giessen, H. Mid-Infrared Fourier-Transform Spectroscopy with a High-Brilliance Tunable Laser Source: Investigating Sample Areas down to 5 Mm Diameter TL - 23. *Opt. Express* **2015**, *23*, 11105−11113.
(50) Klein, M. W.; Wegener, M.; Feth, N.-A.; Linden, S. Experiments on Second- and Third-Harmonic Generation from Magnetic Metamaterials: Erratum. *Opt. Express* **2008**, *16*, 8055.
(51) Metzger, B.; Gui, L.; Fuchs, J.; Floess, D.; Hentschel, M.; Giessen, H. Strong Enhancement of Second Harmonic Emission by Plasmonic Resonances at the Second Harmonic Wavelength. *Nano Lett.* **2015**, *15*, 3917−3922.
(52) Linnenbank, H.; Linden, S. Second Harmonic Generation Spectroscopy on Second Harmonic Resonant Plasmonic Metamaterials. *Optica* **2015**, *2*, 698−701.
(53) Hentschel, M.; Utikal, T.; Giessen, H.; Lippitz, M. Quantitative Modeling of the Third Harmonic Emission Spectrum of Plasmonic Nanoantennas. *Nano Lett.* **2012**, *12*, 3778−3782.
(54) Metzger, B.; Gui, L.; Giessen, H. Ultrabroadband Chirped Pulse Second-Harmonic Spectroscopy: Measuring the Frequency-Dependent Second-Order Response of Different Metal Films. *Opt. Lett.* **2014**, *39*, 5293−5296.
(55) Tsang, T. Y. F. Optical Third-Harmonic Generation at Interfaces. *Phys. Rev. A: At., Mol., Opt. Phys.* **1995**, *52*, 4116−4125.
(56) Cheng, J.-X.; Xie, X. S. Green's Function Formulation for Third-Harmonic Generation Microscopy. *J. Opt. Soc. Am. B* **2002**, *19*, 1604−1610.
(57) Olmon, R. L.; Slovick, B.; Johnson, T. W.; Shelton, D.; Oh, S.-H.; Boreman, G. D.; Raschke, M. B. Optical Dielectric Function of Gold. *Phys. Rev. B: Condens. Matter Mater. Phys.* **2012**, *86*, 235147.
(58) Weiss, T.; Granet, G.; Gippius, N. a.; Tikhodeev, S. G.; Giessen, H. Matched Coordinates and Adaptive Spatial Resolution in the Fourier Modal Method. *Opt. Express* **2009**, *17*, 8051−8061.
(59) Zuloaga, J.; Nordlander, P. On the Energy Shift between near-Field and Far-Field Peak Intensities in Localized Plasmon Systems. *Nano Lett.* **2011**, *11*, 1280−1283.
(60) Alonso-González, P.; Albella, P.; Neubrech, F.; Huck, C.; Chen, J.; Golmar, F.; Casanova, F.; Hueso, L. E.; Pucci, A.; Aizpurua, J.; et al. Experimental Verification of the Spectral Shift between near- and Far-Field Peak Intensities of Plasmonic Infrared Nanoantennas. *Phys. Rev. Lett.* **2013**, *110*, 203902.
(61) Menzel, C.; Hebestreit, E.; Mühlig, S.; Rockstuhl, C.; Burger, S.; Lederer, F.; Pertsch, T. The Spectral Shift between near- and Far-Field Resonances of Optical Nano-Antennas. *Opt. Express* **2014**, *22*, 9971−9982.

DOI: 10.1021/acsphotonics.8b00079
ACS Photonics 2018, 5, 1863−1870